Microstructure characterisation of a high strength steel weld metal containing the novel constituent coalesced bainite

E. Keehan*, H. K. D. H. Bhadeshia **, H.-O. Andrén*,
L. Karlsson*** and L.-E. Svensson*

*Department of Experimental Physics, Chalmers University of Technology,
SE – 412 96 Gothenburg, Sweden.

** University of Cambridge, Department of Materials Science and Metallurgy,
Pembroke Street, Cambridge CB2 3QZ, U.K.

*** ESAB AB, P.O. Box 8004,
SE – 402 77 Gothenburg, Sweden.

Abstract

An experimental high strength steel weld metal containing 7 wt. % nickel and 2 wt. % manganese was found to have a complex microstructure. Employing high resolution characterisation techniques the microstructure consisted primarily of a mixture of martensite, upper bainite and a novel constituent with large grain size that contained plate-like precipitates. This constituent was characterised to have a ferritic matrix with cementite precipitates. Considering morphology, crystallography and recorded phase transformation temperatures it was concluded the novel constituent was a variant of bainite best described as coalesced bainite.

Introduction

The welding of high strength steel has taken place on a limited basis since the 1960's using mainly gas tungsten arc welding [1]. Then weld metals for this technique were developed which gave a combination of high impact toughness at low temperatures and high strength when used with tightly controlled welding parameters. However, for the more flexible and productive welding processes such as shielded metal arc welding (SMAW), flux cored arc welding, or submerged arc welding, the development of weld metals that maintain acceptable impact toughness at low temperatures as yield strength increases above the region of 690 MPa (100 ksi) continues to be the subject of investigation.

Weld metals have been produced for a variety of welding methods with yield strength levels up to and above 1000 MPa but high impact toughness has only been achieved at moderate yield strengths. The microstructures of these weld metals generally are a mixture of ferrite, bainite,

1

martensite or retained austenite [2–10]. To produce these microstructures somewhat different alloying concepts have been used. Mostly, the weld metals contain manganese (1 – 2%), chromium (up to approximately 0.5%), molybdenum (approximately 0.5%) and nickel (up to approximately 4%) [2–9]. In weld metals nickel is usually added to improve the low temperature impact toughness. Nickel does not normally form a carbide; it therefore remains in solid solution and strengthens the ferrite [11–12].

To investigate the effect of nickel further and to possibly improve the impact toughness, the nickel content of a commercial SMAW electrode (Esab OK 75.78) was increased from 3 to 7 %. The welding parameters, chemical composition and tensile properties for this new experimental weld metal are presented in Table 1. Results from Charpy impact toughness testing are presented in Table 2 [14]. This weld metal had good strength but the recorded impact toughness was low which was in line with previous work where an experimental weld metal with 7.45Ni, 1.6Mn and 0.02C was tested [15]. Light optical microscopy (LOM) of the 7.2Ni, 2Mn and 0.03C weld metal revealed a fine scale microstructure, probably consisting of martensite or bainite along with a novel constituent with a very large grain size [14]. This was contrary to the previously reported microstructure in the 7.45Ni, 1.6Mn, 0.02C weld metal where only lath martensite was found [15].

The present work deals with the detailed characterisation of the microstructure using a combination of high resolution experimental methods with a special focus on the previously not recorded constituent. The general morphology of the novel constituent is shown in Figure 1. No knowledge of a constituent with the given morphology has previously been reported in high strength steel weld metals.

	7-2L250
E / kJ mm^{-1}	1.2
IPT / °C	250
$t_{8/5}$ / s	12
C *	0.032
Mn	2.02
Ni	7.23
Cr	0.47
Si	0.25
S*	0.008
P	0.011
Mo	0.63
Cu	0.03
O / ppm*	380
N / ppm*	250
YS / MPa	795
UTS / MPa	1006
YS / UTS	0.79
A5 / %	15

Table 1 Welding parameters and chemical composition. Welding parameters presented are energy input (E), interpass temperature (IPT) and the estimated cooling time between 800 and 500 °C ($t_{8/5}$) calculated from WeldCalc. [13] Composition is in wt. % unless otherwise stated and '*' indicate elements analysed using Leco Combustion equipment.

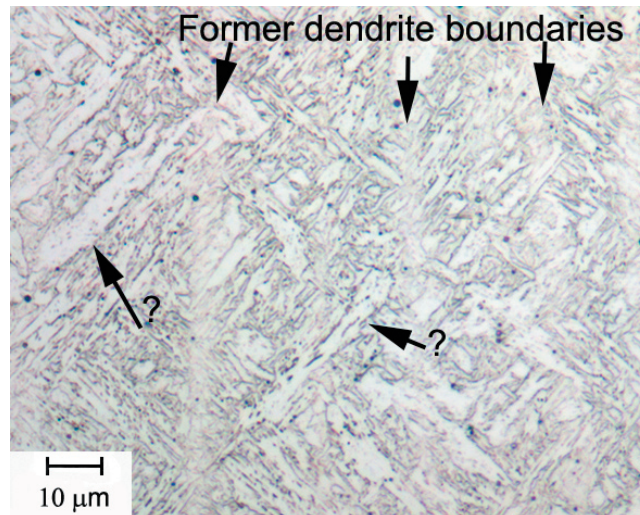| Temp / °C	–80	–60	–40	–20	0	22
Energy / J	12	15	32	38	40	45

Table 2 Charpy–V impact toughness.

Figure 1 LOM micrograph of as-deposited weld metal showing a dendritic microstructure. Also shown are coarse unidentified grains with a "?" .

Experimental Details

The weld joint was made according to ISO 2560 using 20 mm plates with a backing plate. The joint was buttered before deposition of the experimental weld metals which took place in 33 cm runs with two or three runs per layer. The welding parameters are presented in Table 1.

Specimens from the weld metal cross section, extracted perpendicular to the welding direction, were mounted in bakelite for analysis with LOM and field emission gun scanning electron microscopy (FEGSEM). The samples were wet ground, polished to 1 μm diamond grain size and etched using 2 % nital etchant. A Leitz Aristomet LOM along with a Leo Ultra 55 FEGSEM were used in these examinations. For transmission electron microscopy (TEM) studies, 3 mm disc shape samples, perpendicular to the welding direction, were ground to between 50 and 80 μm in thickness. They were then jet electropolished at –35 °C using 10 % perchloric acid in methanol. After electropolishing the specimens were further thinned by ion beam milling for a few minutes at a low angle using a Gatan Precision Ion Polishing System (PIPS). These specimens were examined with a Jeol 2000 FX TEM.

Hollow and solid cylindrical dilatometry specimens were machined from the centre of the welded joint. Hollow specimens with an outer diameter of 4.9 mm, inner diameter of 3.5 mm and length 12.5 mm were used for measurements with cooling rates greater that 50 °C / s. Solid specimens with 3 mm diameter and 10 mm length were used at lower cooling rates. All specimens were analysed using a Theta Dilatronic III dilatometer to record the phase transformation temperatures and to produce a continuous cooling transformation diagram. The specimens were heated up to 1000 °C at a rate of 25 °C / s, held for 5 minutes and then cooled at different rates to room temperature. Individual samples were used for each cooling rate. Following dilatometry, the samples were metallographically prepared and examined in the FEGSEM; the Vickers hardness was measured using a 1 kg load in accordance with EN 112517.

Results

Microstructure of last bead

The former dendrite boundary regions which developed during solidification are clearly visible in the light optical micrograph shown in Figure 1. It seems from the micrograph that a coarser microstructure (of the novel constituent) develops preferentially within the dendrites with mainly a finer lath-like microstructure at the prior dendrite boundaries. Microstructural investigations of the as-deposited last bead, using the FEGSEM, proved to be very revealing. Figure 2 shows a FEGSEM micrograph at a compatible magnification to Figure 1. With this technique it was possible to conclude that the laths had the typical morphology of martensite (Figure 3) while upper bainite and small amounts of lower bainite were mainly found along with the large unidentified grains within the dendrites. These large grains varied in size with up to 4 μm in width and 15 μm in length observed in the sections examined. The higher magnification image shown in Figure 4 reveals plate-shaped precipitates within the novel constituent.

A grain with similar size and morphology as the larger grains observed with LOM and FEGSEM was studied with TEM. A low magnification bright field image giving an overview is shown in Figure 5. Using electron diffraction cementite was confirmed to be present at the grain boundary and also a group of cementite platelets were found to be penetrating the boundary. In Figure 5 it is just about possible to see very small precipitates within the grain. These precipitates are
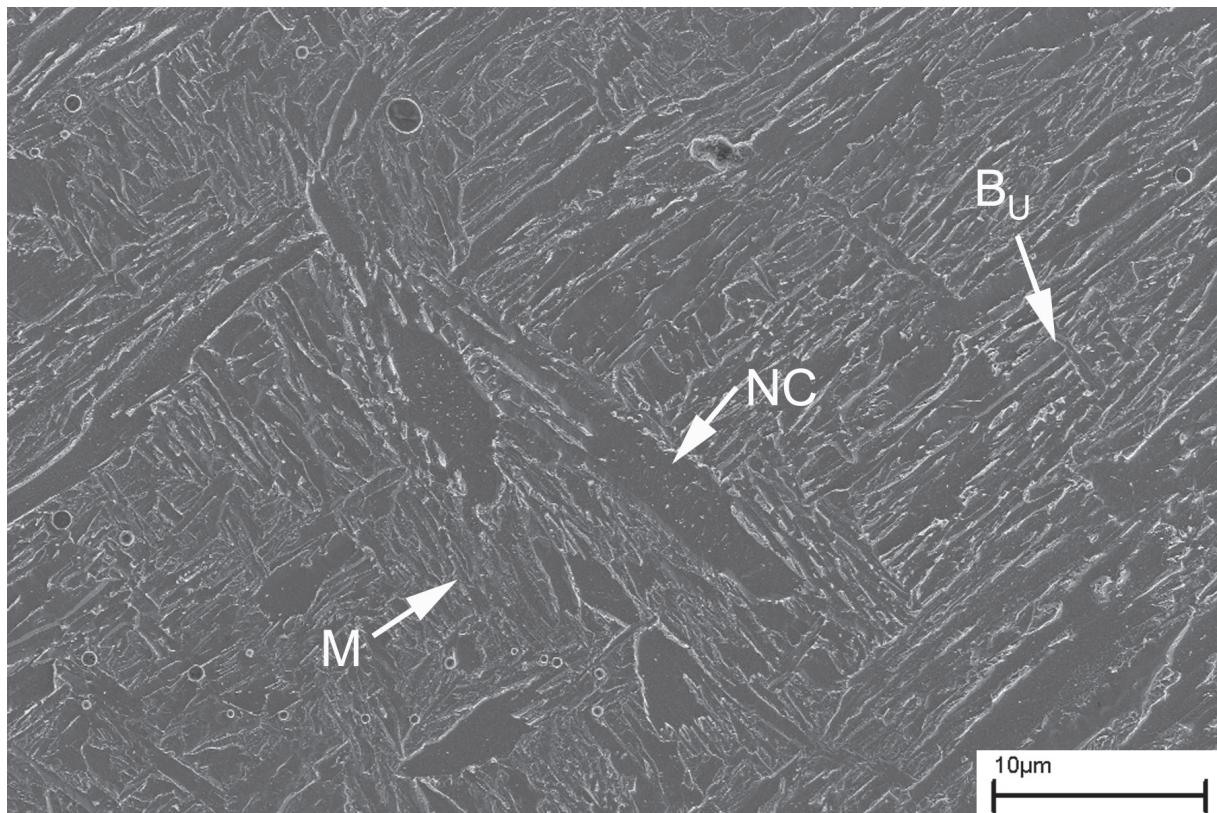

Figure 2 An overview of the as-deposited weld metal microstructure with FEGSEM where M is martensite, B_U is upper bainite and NC is novel constituent.
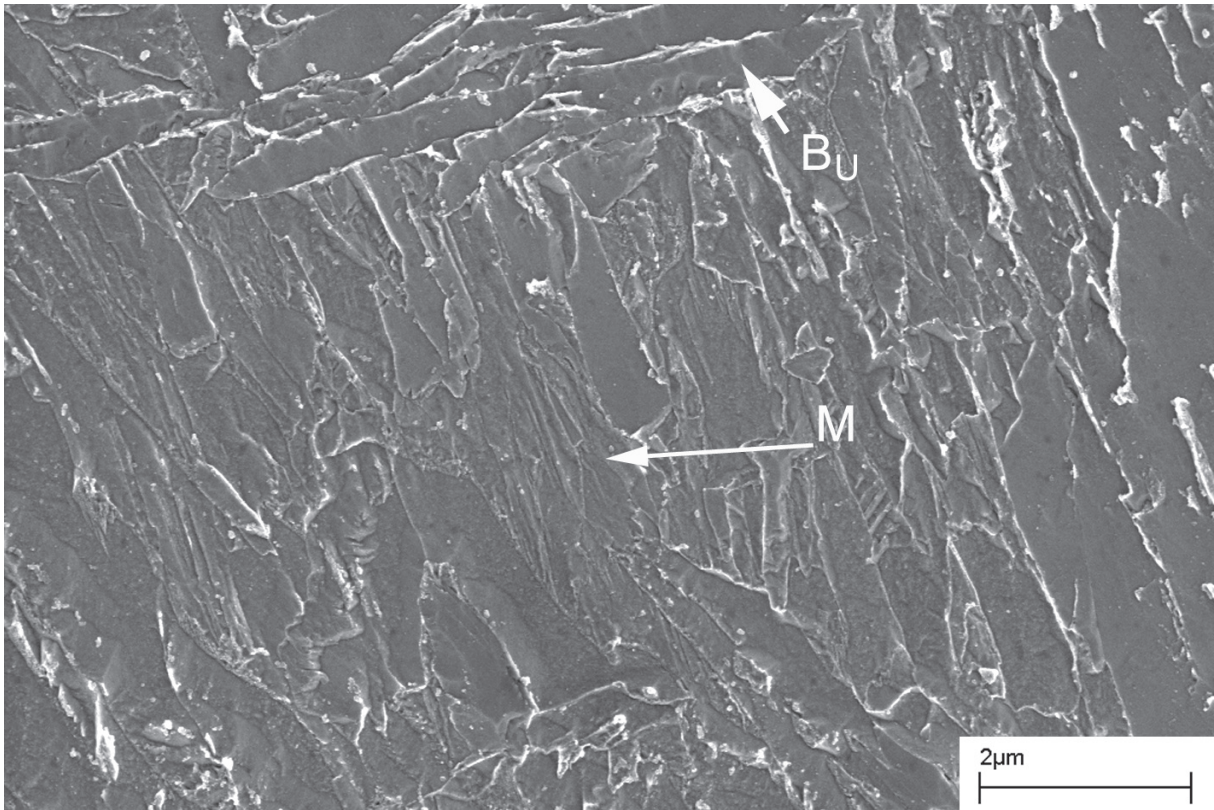
Figure 3 Martensite (M) and upper bainite (B_U) shown at higher magnification using FEG-SEM.
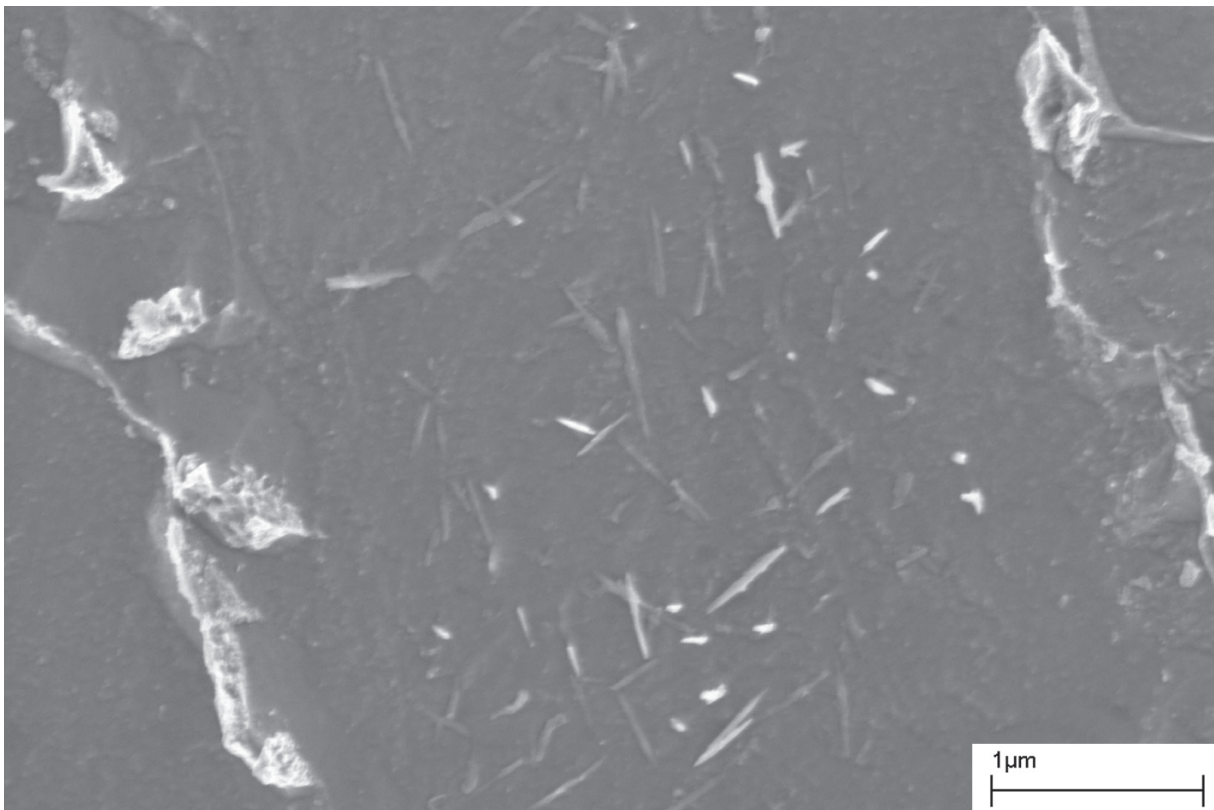

Figure 4 High magnification FEGSEM micrograph showing precipitates within a novel constituent grain in as-deposited weld metal.
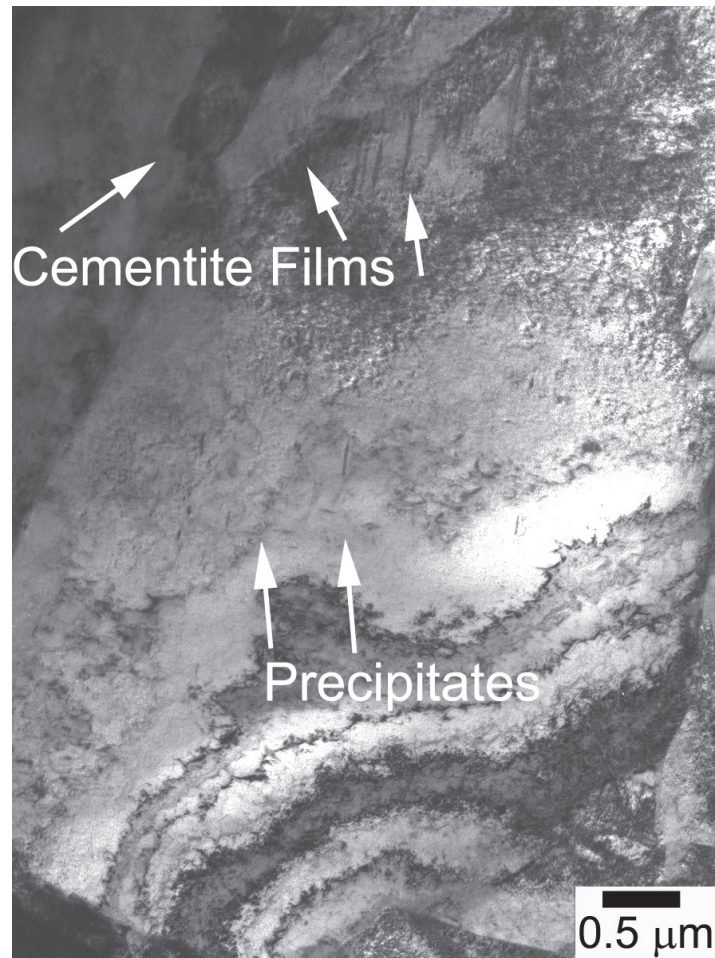
Figure 5 Low magnification bright field TEM micrograph of a larger grain in as-deposited weld metal. Cementite films are visible at the grain boundaries and small plate-like precipitates can be seen within the grain.

Figure 6 Higher magnification bright field TEM micrograph showing the precipitates within the same grain as in Figure 5.
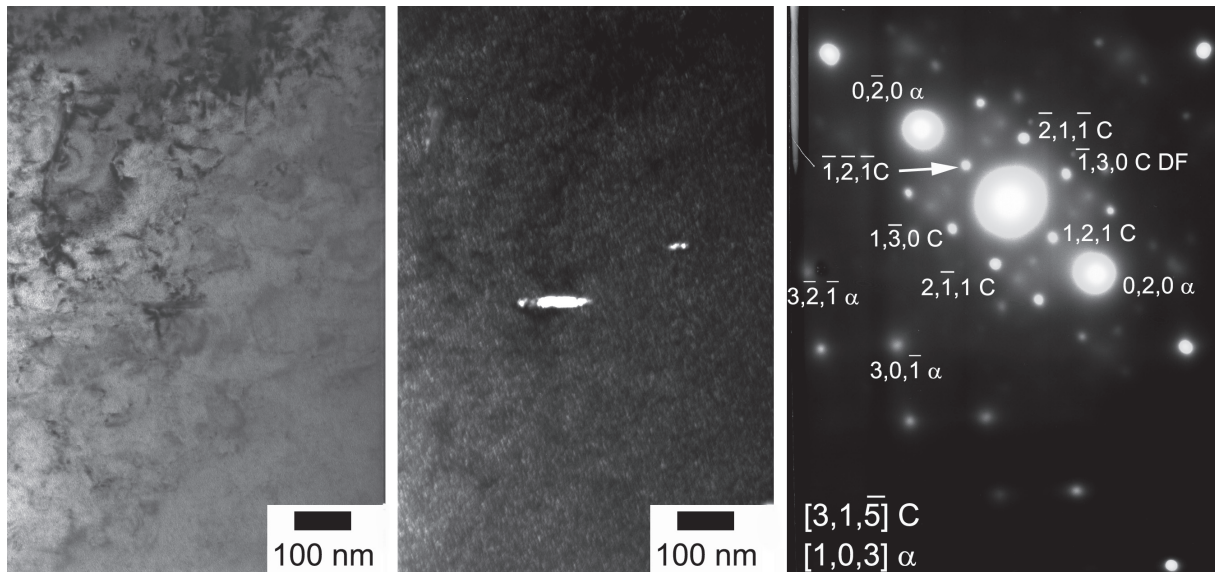
Figure 7 TEM bright (left) and dark (middle) field images with corresponding diffraction pattern (right) of a precipitate within the grain shown in Figure 5. The dark field image was formed using the {−1,3,0} cementite reflection.

shown at higher magnification in Figure 6. Similar precipitates observed with FEGSEM were found to have a plate like morphology and can be up to 0.5 μm in size. The precipitates were confirmed to be cementite with electron diffraction (Figure 7) using documented lattice parameters [16–18]. Additionally, retained austenite was observed with TEM at some lath boundaries in the last bead.

Dilatometry — CCT diagram

A CCT diagram compiled from dilatometry measurements is presented in Figure 8. The Ac_1 and Ac_3 temperatures were measured to be 690 and 740 °C, respectively. Curves A and B represent the fastest cooling rates and it was not possible to decipher the transformation temperatures for these with any confidence due to the limitations of the equipment. For Curve C and D transformation began between 370 and 375 °C while for Curves E and F the transformation temperatures increased slightly to the region of 400 °C. The average hardness of two or three measurements on individual specimens is presented under the related cooling curves.

Dilatometry — Microstructure

Selected results from microstructural investigations with FEGSEM of the dilatometry specimens are presented in Figures 9 – 12. It was found that as the cooling rate decreased, the microstructure changed from that of a very fine scale morphology to one with more coarse grains. Figure 9 shows the microstructure obtained in the dilatometry specimen corresponding to Curve A in Figure 8 which was cooled at a rate of roughly 115 °C / s (measured from 1000 to 300 °C). The specimen was cooled as quickly as possible with the dilatometer and a mainly martensitic microstructure was obtained. As the cooling rate was slowed down to approximately 25 °C / s (Curve C), the microstructure showed a dispersion of distinctly larger grains (Figure 10). Moving to even slower cooling, around 1°C / s (Curve E), it was found that the microstructure
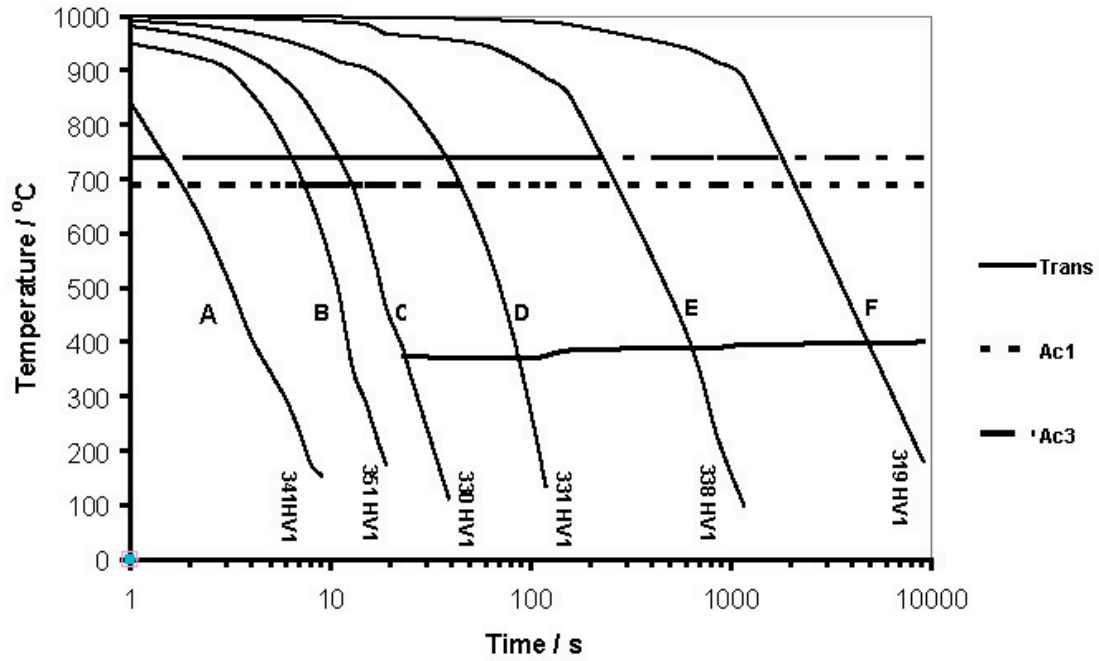
Figure 8 CCT diagram constructed from results of dilatometry experiments. Also plotted is the average result of two or three hardness measurements on each specimen.
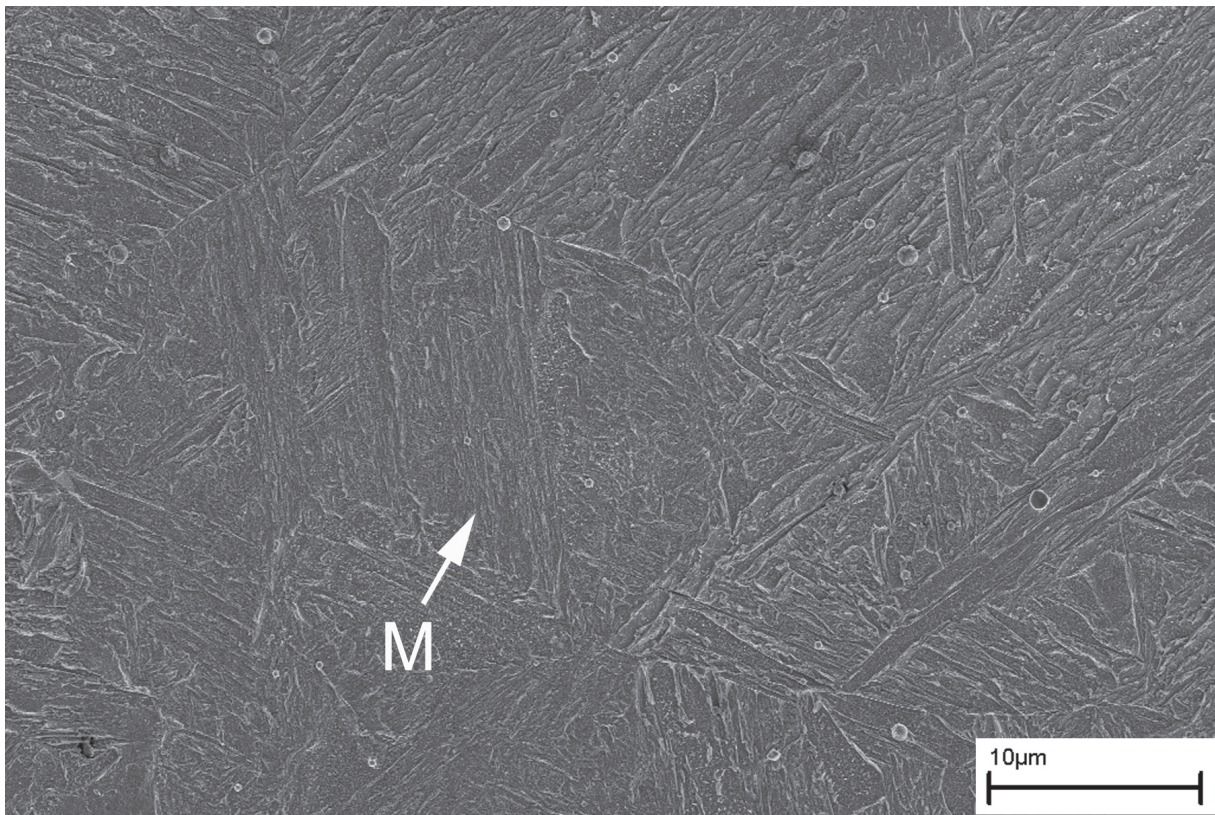

Figure 9 Low magnification FEGSEM micrograph from the dilatometry specimen corresponding to cooling curve A showing a mainly martensitic microstructure. M is martensite.
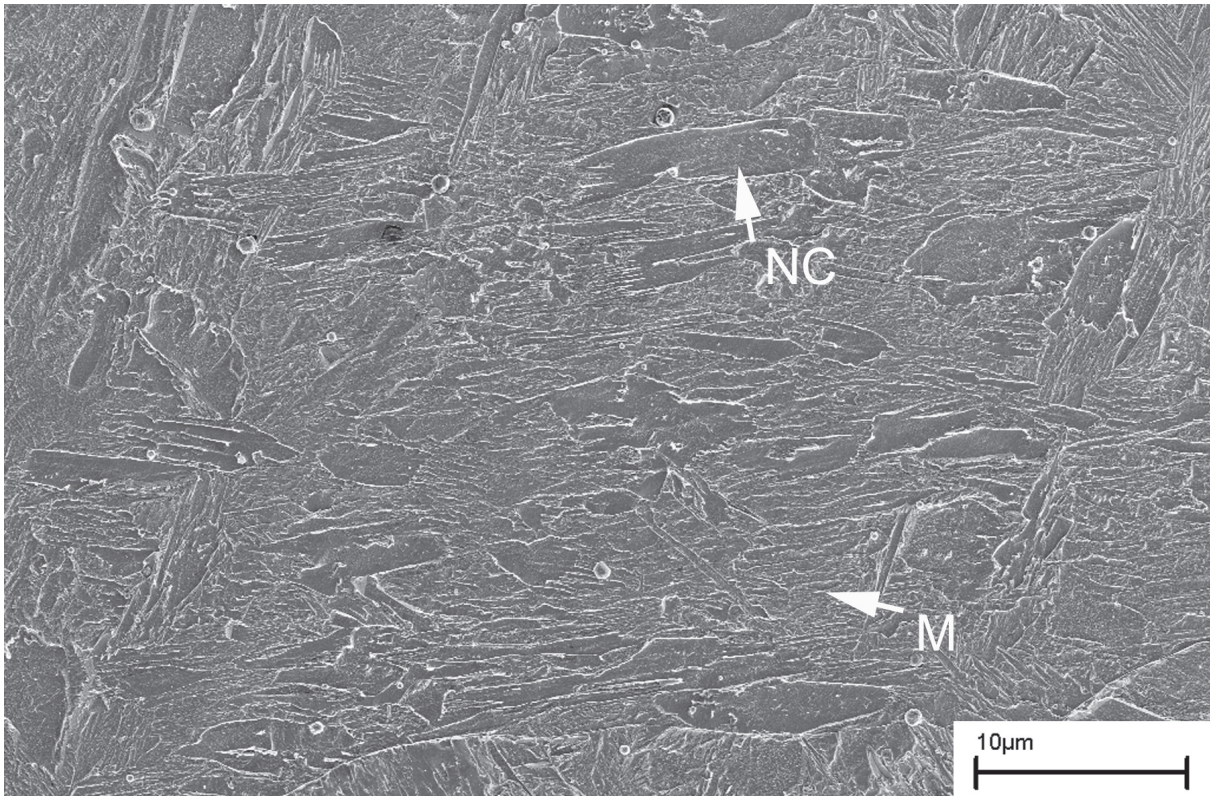
Figure 10 FEGSEM micrograph from the dilatometry specimen corresponding to cooling curve C in Figure 8. The microstructure was found to consist of mainly martensite (M) and large grains of the novel constituent (NC).
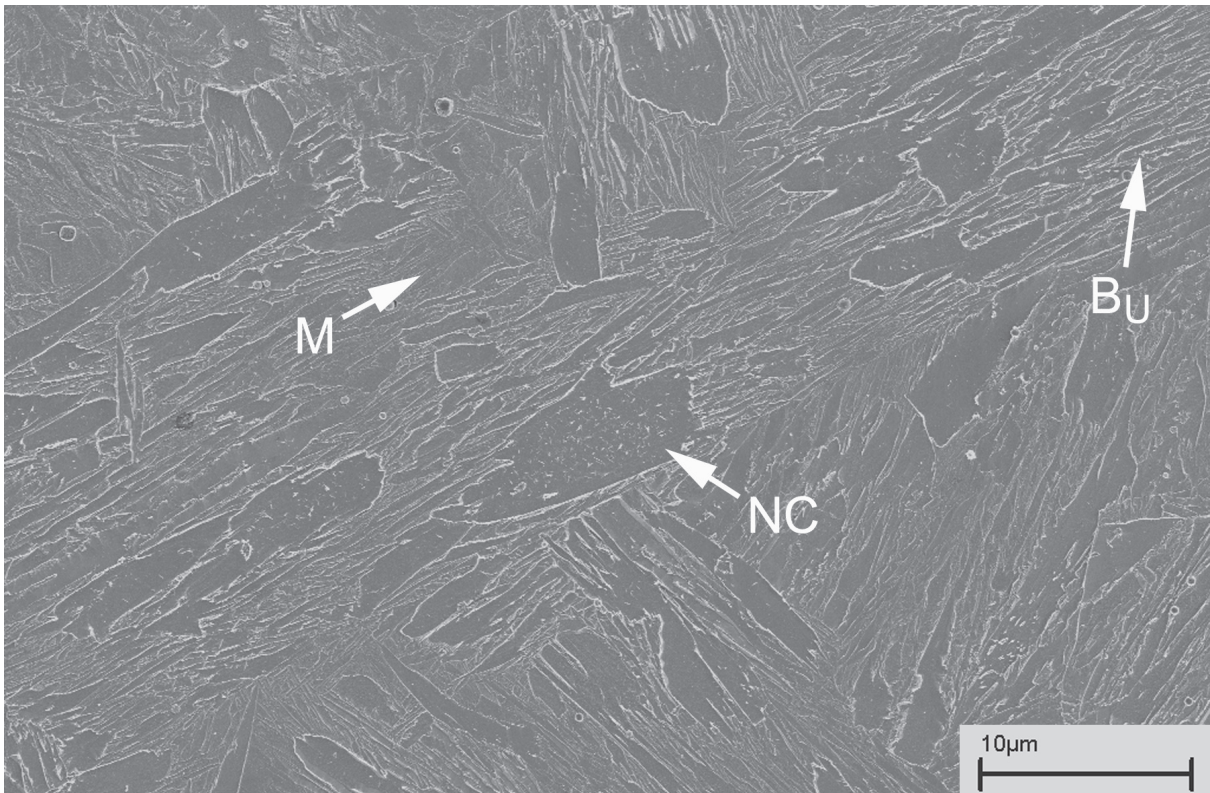

Figure 11 Low magnification FEGSEM micrograph from the dilatometry specimen corresponding to cooling curve E in Figure 8 showing a mixed microstructure. Martensite is M, upper bainite is B_U and novel constituent is NC.
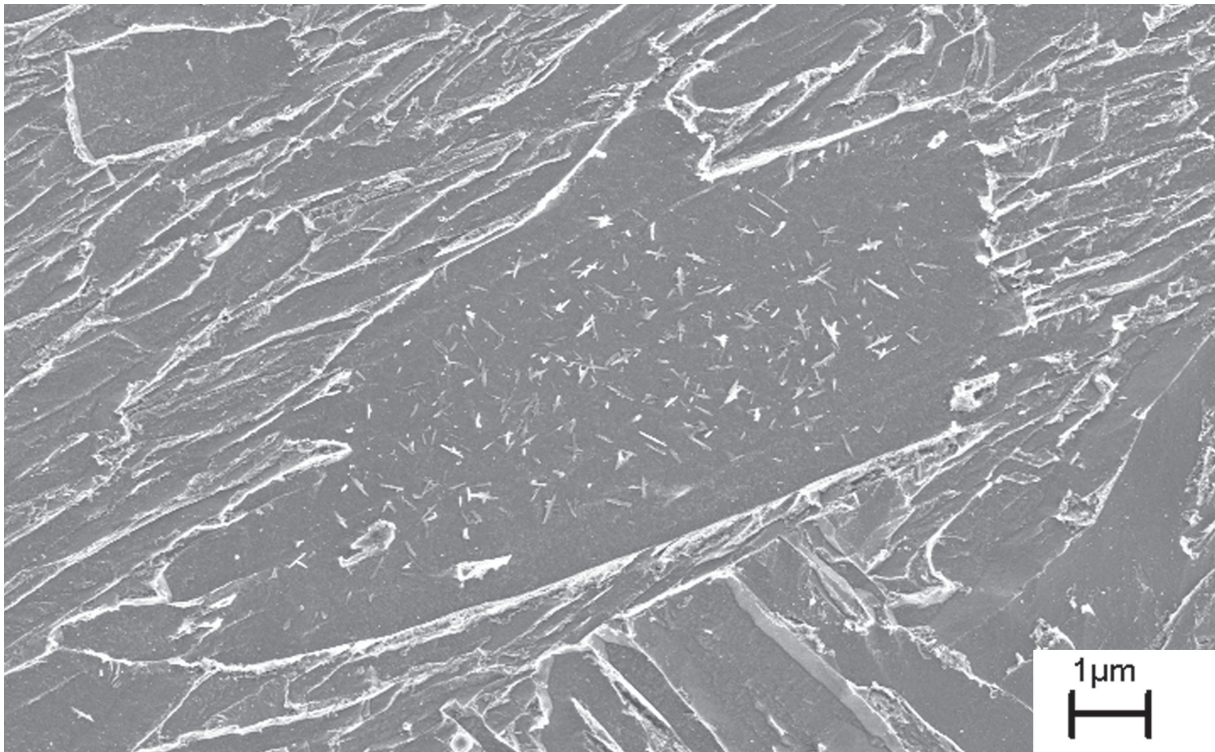
9

Figure 12 FEGSEM micrograph from the dilatometry specimen corresponding to cooling curve E showing the morpology of the novel constituent at higher magnification.

obtained was mainly bainitic with some martensite remaining (Figure 11), together with the unidentified constituent shown on a larger scale in Figure 12.

Discussion

It was only possible to characterise the fine scale microstructure through the use of high resolution instruments such as FEGSEM and TEM. A general conclusion from the combination of experiments is that the as-deposited last bead microstructure is essentially a mixture of martensite, upper bainite and a novel constituent. The latter two are located mainly within the dendrites of the solidification microstructure whereas the martensite is predominantly found at the dendrite boundaries. The interdendritic regions are richer in solute (Ni, Mn, [19]) and hence transform easier into martensite. The upper bainite and the unidentified, coarse grains were located within the dendrites consistent with transformation occurring at a higher temperature. Transmission electron microscopy confirmed the fact that the constituent matrix has a ferrite crystal structure and that the particles within it are platelets of cementite. Furthermore, the cementite particles are present in many crystallographic orientations within the grains.

The question then arises as to whether these grains are autotempered martensite or a variant of bainite. It used to be thought that tempered or autotempered martensite shows many variants of cementite whereas there is only a single variant present in lower bainite. However, it has been shown that this is not generally true and that there are many circumstances where multiple variants occur in lower bainite [21–23] and single variants in martensite [20].

In addition the size of the large grains (up to 13 μm in length and 4 μm in width) is not what one would expect for that of autotempered martensite. It must also be noted that these large grains formed as single units since no former lath boundaries were observed within the large grains (Figures 5 and 6). Also since the transformation temperature was low (< 400 °C), it would not be possible to remove traces of lath boundaries even if they did previously exist.

Finally, the clearest evidence against the constituent being autotempered martensite is that its fraction increases as the cooling rate decreases. The temperature at which martensite forms (autotempered or otherwise) is not affected by cooling rate in steels (or weld metals) of the type considered here. Furthermore, the fraction of martensite is only a function of the undercooling below the martensite-start temperature and not the rate at which that temperature is reached. Taking all these points into consideration it can be strongly suggested that the observed large grains are those of a novel variant of bainite rather than martensite.

When the morphology of the large grains are observed carefully, its transformation front is found to consist of a series of finer platelets, all in identical crystallographic orientation, which coalesce at some distance behind the advancing tips to generate the observed coarse grains. This phenomenon was observed in Figure 12 and has been previously reported where lower bainite was studied [24–25]. When many identically oriented plates are nucleated, they can coalesce into a thicker plate if the undercooling is large enough to sustain the strain energy [24–25]. As temperature drops, within the centre of the large grains, carbon precipitates to several families of cementite while close to the boundaries carbon diffuses to the boundaries leaving a precipitate free zone. A schematic representation of the growth of coalesced bainite is presented in Figure 13 along with that of upper and lower bainite.

The transformations occur at a large undercooling below Ac_3 and therefore are associated with large driving forces consistent with rapid nucleation and growth. In literature it is reported that nucleation rate of lower bainite is large at temperatures close to M_S [24]. The B_S and M_S temperatures have been estimated using empirical equations [26–27] and the average composition of the weld metal (Table 1) to be 287 °C and 326 °C respectively. After allowing for the effect of chemical segregation [19] the transformation temperatures at the dendrite centres, where the novel constituent forms the transformation temperatures become 341 °C and 349 °C respectively. These predictions are not expected to be accurate since the equations do not extend to large nickel concentrations, but they are consistent with the observed transformation temperatures in the CCT diagram (Figure 8).

It is not possible at this stage to conclude that the coalesced bainite is detrimental to mechanical properties, but it may well have an influence given that it presents large regions of identical crystallography to propagating cracks. Further discussions in relation to mechanical properties are presented elsewhere [29]
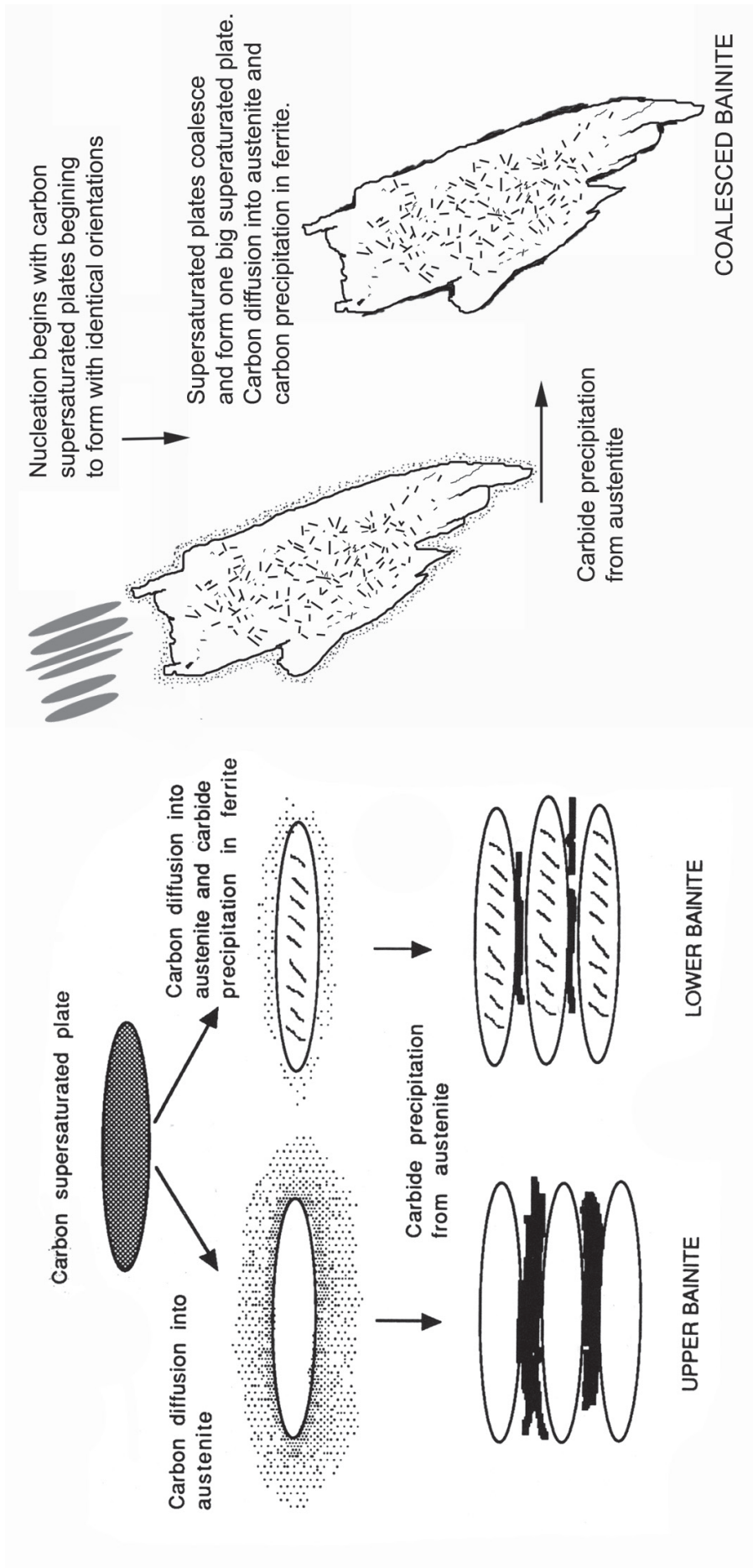
Figure 13 Schematic representation of the formation of upper and lower bainite [28] along with coalesced bainite based on Figure 12.

Conclusions

The microstructure of an experimental weld metal with 0.03C, 7Ni and 2Mn was characterised using TEM, FEGSEM and LOM and found to consist of a mixture of martensite, upper bainite and a previously not reported constituent. The novel constituent appears to arise through the coalescence of bainitic ferrite plates in identical crystallographic orientation. It forms with an increasing tendency as the cooling rate from the austenite phase field is reduced. The novel constituent is concluded to be that of coalesced bainite. The coalesced bainite is believed to be detrimental to toughness and is the subject of further work presented elsewhere.

Acknowledgements

References

1. D.J. Widgery, L. Karlsson, M. Murugananth & E. Keehan, Approaches to the development of high strength weld metals, Proceedings 2nd Int. Symposium on High Strength Steel, Norway (2002).
2. J.F. Deloach: Proceedings, International Conference on Welding Technology, Material and Fracture, (1990), Geesthacht, Germany: Gournay-sur-Marne, France; IITT International; 1990.
3. P.R. Oldland, C.W. Ramsay, D.K. Matlock, D.L. Olson: Welding Journal, 68, April, (1989), p. 158.
4. M.G. Vassilaros, E.J. Czyryca: Proceedings, Advances in Low-Carbon High Strength Ferrous Alloys (LCFA-92), Jamshedpur (India), March 25–28, (1992): Key Engineering Materials (Switzerland).
5. D.B. Fleming, A.Q. Bracarense, S. Liu, D.L. Olson: Welding Journal (USA), 75 June (1996), p. 171.
6. D.E. McRobie, J.F. Knott, Materials Science and Technology, 1 May (1985), p. 357.
7. L.-E. Svensson, B. Gretoft: Welding Journal, 69 December (1990), p. 454.
8. T.W. Lau, M.M. Sadowsky, T.H. North, G.C. Weaterly: The Metallurgical Society / AIME, 1987 p. 349.
9. L.-E. Svensson: Svetsaren, 54, January (1999).
10. M. Lord: Design and Modelling of Ultra - High Strength Steel Weld Deposits, Ph. D. Thesis, (1999), University of Cambridge: Cambridge.
11. L.-E. Svensson: Control of microstructure and properties in steel arc welds, CRC Press, Inc (1994) p 69

12. ASM: Properties and Selection Iron, Steel and High Performance Alloys. 10th Ed. ASM Handbook. Vol. 1 (1990).

13. SSAB Oxelösund, WeldCalc, Version 1.0.0, 98 – 99.

14. E. Keehan, H. O. Andrén, L. Karlsson, L.-E. Svensson, New developments with C–Mn–Ni high strength steel weld metals, Part B. Mechanical Properties, In manuscript.

15. Y. Kang, H.J. Kim, and S.K. Hwang: ISIJ International (Japan), 40 December (2000), p. 1237.

16. K.W. Andrews, D. J. Dyson, S. R. Keown, Interpretation of Electron Diffraction Pat terns, 2nd Ed., Adam Hilger Ltd., London (1971).

17. J. W. Edington, Practical Electron Microscopy in Material Science, The Macmillan Press Ltd., London (1975)

18. http://cimesg1.epfl.ch/CIOL/ems.html

19. E. Keehan, H. O. Andrén, L. Karlsson, M. Murugananth, H. K. D. H. Bhadeshia, Microstructural and mechanical effects of nickel and manganese on high strength steel weld metals, 6th Int. Conference on Trends in Welding Research, pp. 695–700, Pine Mountain, Georgia, USA, April 15–19, 2002.

20. H.K.D.H. Bhadeshia, Bainite in Steels, 2nd. Ed., IOM communications Ltd., London, 2001, Chapter 8.

21. G. R. Srinivasan and C. M. Wayman, Acta Metall., 16 (1968) pp 602–609.

22. G.Y. Lai, Metall. Trans. A **6** A (1975) 1469

23. H.K.D.H. Bhadeshia and D. V. Edmonds, Metall. Trans. 10 A (1979) pp 895–907

24. H.K.D.H. Bhadeshia, Bainite in Steels, 2nd. Ed., IOM communications Ltd., London, 2001

25. H.K.D.H. Bhadeshia, Theory and Significance of Retained Austenite in Steels, Ph.D. thesis, University of Cambridge, 1979

26. R.W.K. Honeycombe, H.K.D.H. Bhadeshia, Steel Microstructure and Properties, 2nd Ed., Edward Arnold, London, 1995, p 133

27. R.W.K. Honeycombe & H.K.D.H. Bhadeshia, Steel Microstructure and Properties, 2nd Ed., Edward Arnold, London, 1995, p 103

28. M. Takahashi, H.K.D.H. Bhadeshia, Materials Science and Technology, 6 (1990) pp. 592 – 603.

29. E. Keehan, L. Karlsson, H.-O. Andrén, L.-E. Svensson, New developments with C–Mn–Ni high strength steel weld metals, Part B. Mechanical Properties, In Manuscript